RSC Advances

PAPER

View Article Online
View Journal | View Issue

Cite this: *RSC Adv.*, 2025, **15**, 32071

Solvent-free fabrication of TPU-reinforced PE/carbon composites for high-performance positive temperature coefficient materials in lithium-ion battery safety

Yang Lyu, * ZiQian Xiang, LuoJia Chen, Zuo Sheng Li, Jiangfeng Wang, Kuo Chen, Daofa Ying, BaoHui Chen and ChuanPing Wu

Positive temperature coefficient (PTC) materials are pivotal for safeguarding lithium iron phosphate batteries, yet their industrial application is hindered by critical drawbacks: excessive film thickness, high internal resistance, and poor solvent sustainability. Addressing these challenges, this study innovatively develops a solvent-free thermal rolling process to fabricate an asymmetric expansion polymer film, specifically thermoplastic polyurethane (TPU) reinforced polyethylene (PE)/carbon composites, which significantly enhances the PTC effect. The core mechanism lies in the asymmetric thermal expansion of TPU and PE: this unique behavior disrupts the conductive carbon network, triggering a sharp PTC transition at around 120 °C. Further validation *via* an electrochemical-thermal coupling model confirms that the abrupt resistance increase effectively terminates battery discharge, a key safety function. The optimized composite (1% TPU-1% C@PE) exhibits exceptional performance: it features an ultrathin structure (8.5 μm) with low resistance (78 Ω) at room temperature, while reaching a high-resistance state (10 380 Ω) at 120 °C, achieving an impressive resistance ratio of 133.1. Notably, this performance is achieved without compromising the battery's cycling stability. The open circuit voltage of the 1% TPU-1% C@PE battery can quickly drop to 2.5 V within 570 s in an environment of 160 °C, due to the PTC effect. This work not only overcomes long-standing industrial bottlenecks but also provides a practical, scalable strategy, paving the way for advanced safety in lithium battery technology.

Received 15th July 2025
Accepted 27th August 2025

DOI: 10.1039/d5ra05056a

rsc.li/rsc-advances

1 Introduction

In recent years, China's lithium battery energy storage industry has shown a rapid development trend. The new installed capacity reached 168 GWh in 2024, a year-on-year increase of 130%, accounting for more than 97% of the new scale of new energy storage.[1–3] It is expected that the installed capacity will climb to 600 GW and the market scale will exceed 2 trillion yuan by 2035.[4–6] However, the currently mainstream lithium iron phosphate-graphite system prismatic aluminum shell batteries are prone to trigger internal chain exothermic reactions under extreme thermal, electrical, or mechanical stresses, forming a positive feedback loop of "heat-temperature-reaction", which ultimately leads to thermal runaway and fire explosion accidents.[7] This safety hazard has triggered multiple major accidents worldwide: South Korea has seen more than 30 energy storage station fires since 2017; in 2021, the "Victorian Big Battery" project in Australia suffered a four-day fire due to a fire in the Tesla Megapack system, and the same year, the explosion accident at the Fengtai energy storage station in Beijing caused the sacrifice of two firefighters; in May 2024, the fire at the Gateway energy storage station in the United States took nearly two weeks to be controlled.[8] These accidents show that the thermal runaway problem of lithium batteries has become a key scientific problem restricting the safe development of the energy storage industry, and in-depth research and effective prevention and control are urgently needed.[9–11]

To prevent thermal runaway explosions of lithium-ion batteries, almost all battery cells are equipped with pressure limiting valves to timely discharge the electrolyte vapor and flammable gases generated by thermal runaway of battery cells, thus preventing battery explosions.[12,13] However, the explosion-proof valve can only take effect at the end stage of thermal runaway and cannot stop the chain reaction process of battery thermal runaway during the thermal runaway process.[14,15] Thermal runaway of single cells will still cause fire and explosion accidents due to system thermal propagation.[16,17] To improve the safety of the battery itself, it is urgent to autonomously respond to heat during the battery thermal runaway process to cut off the internal ion or electron transport process and terminate the battery thermal runaway reaction. The current battery thermal safety management mainly uses positive temperature coefficient

State Key Laboratory of Disaster Prevention & Reduction for Power Grid, Changsha, China. E-mail: lv_yang@buaa.edu.cn

(PTC) materials to cut off the electron conduction process of the electrode during the thermal runaway reaction. PTC is realized through two main mechanisms: (1) the destruction of the conductive network during the thermal expansion of the polymer substrate; (2) the decrease in conductivity of the conductive polymer during the ion doping/dedoping process under heating.[18,19] Among them, the thermal expansion of the polymer substrate to destroy the conductive network has obvious cost advantages and compatibility with the manufacturing process of lithium-ion batteries, which can ensure the effectiveness of the PTC materials. At present, according to the type of conductive particles, PTC materials can be divided into metal particle types[20–22] and conductive carbon material types.[23–26] At present, such materials can block abnormal currents through conductor–insulator transitions under internal short-circuit heating conditions, which significantly enhances the safety performance of batteries. However, although PTC materials have been successfully verified in concept since the 2010s, industrial applications still face two major challenges: (1) some polymer substrates are difficult to dissolve, and the polymer has high cohesive energy. The film formed by solution casting has a large thickness, resulting in high battery internal resistance; (2) the dissolution process uses high-boiling-point solvents, which have poor environmental protection and economy. To achieve the integration of PTC materials in commercial batteries, it is necessary to develop manufacturing technologies and process solutions that are fully compatible with large-scale production processes.[27]

Herein, this study innovatively developed an intelligent polymer film based on solvent-free hot rolling process. The thermoplastic hot rolling process using PE/TPU composite system significantly improves the uniformity and mechanical properties of the film while completely avoiding the use of organic solvents. By precisely regulating the asymmetric thermal expansion characteristics of PE and TPU, the composite material prepared can efficiently destroy the conductive carbon network near the critical temperature of 120 °C, thereby significantly enhancing the positive temperature coefficient (PTC) effect. Based on the mutual verification of electrochemical thermal coupling finite element simulation and experimental data, this study deeply reveals the dynamic evolution law of electronic conduction circuit resistance in charging and discharging cycles and its regulation mechanism on battery voltage. This intelligent response film can quickly trigger circuit protection function when the battery overheats, providing a reliable solution for preventing thermal runaway of lithium-ion batteries.

2 Experiment

2.1 Materials and machines

Low-density polyethylene (PE) and thermoplastic polyurethane (TPU) are purchased from Guangdong Lingbo New Material Technology Co., Ltd, the conductive carbon is purchased from IMERYS. Lithium iron phosphate (LFP) is purchased from Hunan Yuneng New Energy Battery Materials Co., Ltd, and graphite is purchased from Hunan Rongli New Material Technology Co., Ltd The corresponding masses of LDPE, TPU, and conductive carbon black are continuously rolled at 100 °C using a thermal rolling mill (GRS-DG300, Shenzhen Kejing Zhida Technology Co., Ltd) to ensure uniform dispersion of the conductive agent and polymer substrate. Subsequently, the rolling pressure is adjusted to 10 tons, and different rolling speeds are set to obtain PTC material films with different thicknesses. The PTC material films with different thicknesses are combined with carbon-coated aluminum foil to prepare current collector materials for batteries.

The positive electrode of the battery is composed of 95 wt% lithium iron phosphate, 3 wt% conductive carbon black, and 2 wt% PVDF, with PE membrane as the separator. The negative electrode consists of 95.5 wt% graphite, 3 wt% conductive carbon black, and 1.5 wt% binder. The electrode materials are prepared by mixing LFP, conductive carbon black, and PVDF powders, and dispersing them in *N*-methylpyrrolidone (2.4 mL solvent per 1 g dry component) using a homogenizer (104 rpm, 10 min) from Shenzhen Kejing Zhida Technology Co., Ltd. The slurry is coated onto aluminum foil or polymer-coated aluminum foil using a blade coater, followed by vacuum drying at 80 °C for 24 h. The cathode materials are cut into 12 mm discs and assembled into CR2032 button cells with 14 mm lithium sheet discs and 14 mm PE separators. Each cell uses an EC: DEC = 1 : 1 LiPF6 solution (0.06 mL, 1 mol L^{-1}) as the electrolyte.

2.2 DFT calculations

The interactions between PE and TPU are investigated using density functional theory (DFT). The ωB97X-D functional (with dispersion correction) and the 6-31G (d, g) basis set are employed to optimize the geometries and calculate interaction energies. The basis set superposition error (BSSE) for interaction energies is corrected by the counterpoise method. Due to the high molecular weight of polyethylene (PE), a truncated alkane chain is used to represent the PE segment, while a single diphenylmethane diisocyanate molecule is employed to model the TPU segment. The interaction energy (ΔE_c) is calculated as the difference between the energy of the PE-TPU complex and the sum of the energies of the isolated PE and TPU monomers, corrected for BSSE:

$$\Delta E_c = (E_A + E_B) - E_{AB} - E_{BSSE}$$

where E_A and E_B represent the energies of the PE and TPU, E_{AB} is the energy of the complex formed by A and B, and E_{BSSE} is the energy of the BSSE correction, and ΔE_c indicates attractive interactions between PE and TPU.

2.3 Finite element study

This paper takes the 280 Ah prismatic aluminum-shell lithium iron phosphate-graphite battery from State Grid Hunan Electric Power Co., Ltd as the research object. The battery is composed of 60 electrode pairs stacked, with the positive and negative electrode sheets sized 165 × 188 mm and 167 × 191 mm, respectively, and the separator sized 194 mm. The 280 Ah battery consists of 4 stacked cores, each with 56 positive tabs and 57 negative tabs. In COMSOL Multiphysics software, the

chemical, electrochemical reactions, and mass transport processes of a single cell are modeled using a three-dimensional electrochemical-thermal coupling Newman model based on the homogeneous porous electrode theory and electrochemical principles.

2.3.1 The mass transfer and current conservation equations in homogeneous porous electrodes.

$$\frac{\partial \varepsilon_l c_l}{\partial t} + \nabla J_l = R_l$$

$$J_l = -D_{l,\mathrm{eff}} \nabla c_l + \frac{i_l t_+}{F}$$

$$i_l = -\sigma_{l,\mathrm{eff}} \nabla c \varphi_l + -\frac{2\sigma_{l,\mathrm{eff}} RT}{F}\left(1 + \frac{\partial \ \ln \ f}{\partial \ \ln \ c_l}\right)(1 + t_+)\nabla \ln \ c_l$$

$$R_l = -\sum_m \frac{v_{\mathrm{Li}+,m} i_{v,m}}{F} - \frac{v_{\mathrm{Li}+} i_{v,\mathrm{dl}}}{nF} + R_{l,\mathrm{src}}$$

$$\nabla i_l = i_{v,\mathrm{total}} + Q_l$$

$$\nabla i_s = \sigma_{l,\mathrm{eff}} \nabla \varphi_s$$

$$D_{l,\mathrm{eff}} = \epsilon_l D_l$$

$$\sigma_{l,\mathrm{eff}} = \epsilon_l \sigma_l$$

$$\sigma_{s,\mathrm{eff}} = \epsilon_s \sigma_s$$

$$i_{v,\mathrm{total}} = \sum_m i_{v,\mathrm{m}} + i_{v,\mathrm{dl}} - \frac{v_{\mathrm{Li}+} i_{v,\mathrm{dl}}}{nF} + R_{l,\mathrm{src}}$$

c_l is the lithium-ion concentration. $D_{l,\mathrm{eff}}$ is the effective lithium ion diffusion coefficient in the electrolyte. i_l is the current in the solution. $\sigma_{l,\mathrm{eff}}$ is the effective electrical conductivity of the solution. σ is the electrical conductivity of the solution. ϵ_l is the volume fraction of the liquid phase. ϵ_s is the volume fraction of the solid phase. J_l is the flux of the electrolyte. t_+ is the transference number of lithium ions in the solution. i_l is the current in the electrolyte. i_s is the current in the solid particles.

2.3.2 The kinetics of lithium-ion intercalation reaction.

$$\eta = E_{ct} - E_{eq}$$

$$E_{ct} = \varphi_s - \varphi_l$$

$$i_{loc} = i_0\left(\exp\left(\frac{\alpha_a F\eta}{RT}\right) - \exp\left(\frac{-\alpha_c F\eta}{RT}\right)\right)$$

η is the overpotential. E_{eq} is the equilibrium potential. E_{ct} is the actual potential. i_{loc} is the local current source. i_0 is the limiting exchange current. α_a and α_c are the transfer coefficients of anodic and cathodic electrode reactions, respectively. F is the Faraday constant, $F = 96\,485$ C mol^{-1}. R is the ideal gas constant, $R = 8.3143$ J (mol^{-1} K^{-1}). T is the temperature.

2.3.3 Lithium diffusion following Fick's second law of diffusion.

$$\frac{\partial c_s}{\partial t} = \nabla(D_s \nabla c_s)$$

$$\left.\frac{\partial c_s}{\partial r}\right|_{r=0} = 0, \quad -D_s \left.\frac{\partial c_s}{\partial r}\right|_{r=r_p} = \sum_m \frac{v_{\mathrm{Li}^+,m} i_{v,m} r_p}{n_m F 3\varepsilon_s}$$

c_s is the lithium-ion concentration in the solid phase. D_s is the diffusion coefficient of lithium ions in the solid phase. r_p is the radius of the solid particle.

3. Results and discussions

Finite element model based on electrochemical thermal coupling was used to verify the effect of collector resistivity change on battery charge discharge curve. A grid independence study reveals that heat generation power converges to ~20 700 W m^{-3} as grid size increases. In order to balance computational efficiency and simulation accuracy, we selected a model containing 6512 units for subsequent simulation analysis. It should be pointed out that relatively sparse grid partitioning may introduce numerical errors, which to some extent affect the accuracy of the results. The trade-off in this method is based on the balance between current computing resources and accuracy requirements. It is recommended that future research adopt finer grid partitioning to further validate the results. For experimental validation, a 280 Ah laminated battery undergoes charge–discharge cycles in a temperature-controlled chamber. After full charging at 1.0 C and a 0.5-hours rest, discharge at 1.0 C records voltage profiles. Fig. 1c demonstrates excellent consistency between simulated and experimental results, confirming model accuracy. The dominance of ohmic polarization under high-current operation manifests through two key effects: (1) significant depression of discharge voltage plateaus and (2) capacity loss due to premature voltage cutoff, confirmed in our simulations. Specifically, increasing electrode resistivity from 3.774 × 105 to 0.944 × 104 mS cm^{-1} exacerbates voltage polarization from 3251 to 2739 mV and causes 94.15% capacity loss. These findings align with Newman's model predictions. This shows that if the resistance of the collector can be increased at high temperature, the discharge reaction process of the battery can be significantly cut off, and the safety of the battery in the process of thermal runaway can be greatly improved.

The positive temperature coefficient (PTC) effect at elevated temperatures can be realized through blending conductive agents with polymers. Currently, the majority of research employs organic solvent casting methods to prepare PTC film materials. However, this approach exhibits notable limitations. Certain polymers possess high cohesive energy, making it difficult to control film thickness during solvent casting, resulting in PTC materials with substantial electrical resistance,

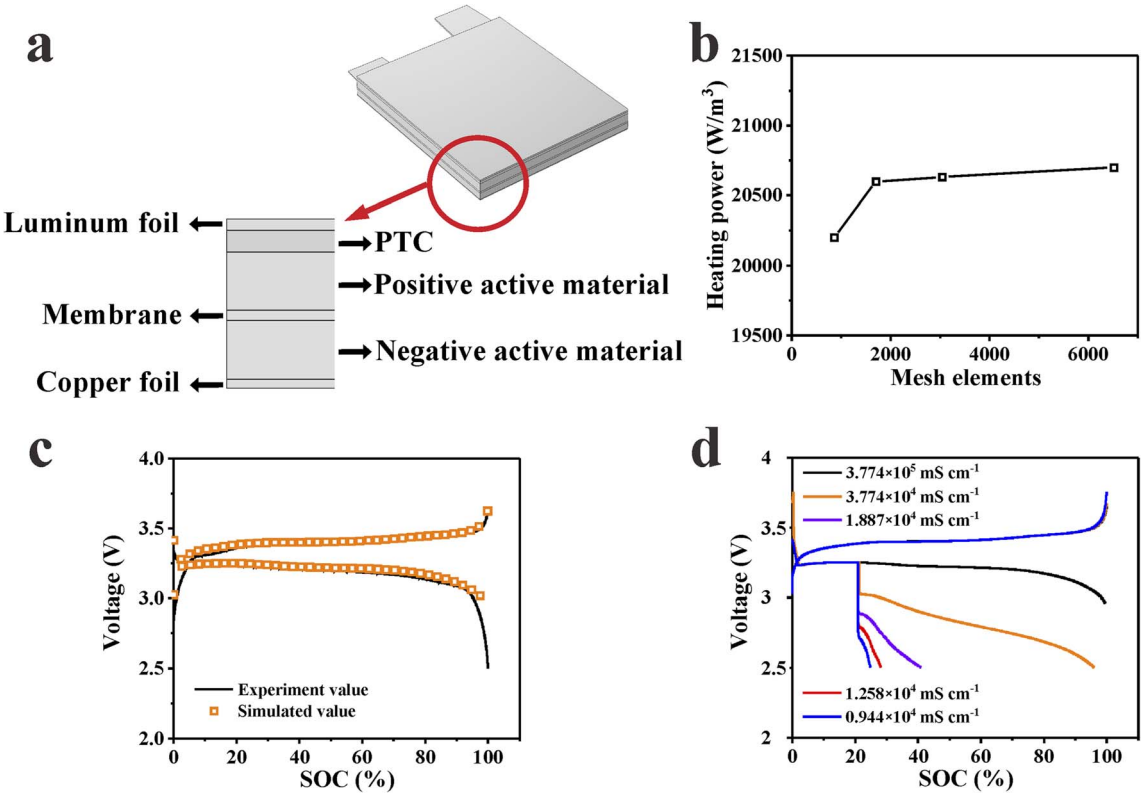

Fig. 1 (a) Electrochemical thermal coupling finite element model. (b) Grid independence study. (c) Charge discharge curves comparison at 1.0 C rate. (d) The effect of electrode conductivity on charging–discharging curve of battery model.

where some solvent-cast films can reach up to 100 μm in thickness. Additionally, the evaporation of organic solvents raises environmental and health concerns while significantly increasing costs. Common solvents such as chloroform, toluene, and DMF may pose carcinogenic or neurotoxic risks, requiring stringent protective measures during processing. In this work, we developed a solvent-free hot-pressing technique using thermoplastic polyethylene (PE) and TPU resin to fabricate PTC materials measuring 8.5 μm in thickness and 100 mm in width. Fig. 2a shows the hot-rolling mill and the PTC material undergoing rolling compression. The rolling mill provides 10 tons of pressure and a thermal field up to 200 °C, with the hot-pressing temperature set at 150 °C. By adjusting the roller speed, the thickness of the 1% TPU-1% C@PE composite could be precisely controlled. Reducing the rolling speed from 1 m min^{-1} to 0.05 m min^{-1} extended the heating duration, facilitating the reduction of intermolecular cohesive forces and decreasing the material thickness from 80 μm to 8.5 μm by prolonging thermal exposure, facilitating polymer chain rearrangement and uniform compression under 10-ton pressure. The PTC material is subsequently cut into 4 × 4 cm squares (Fig. 2c). Micrometer measurements confirm a uniform thickness of 8.5 μm, while the material exhibits ease of processing (Fig. 2c). During the thickness measurement experiment in Fig. 2d, The PTC materials exhibit a bending behavior due to the influence of its own weight. The PTC material inherits the excellent flexibility of polyethylene material. Comparing to conventional solvent casting methods, this approach not only achieves thinner films but also significantly reduces the overall internal resistance and manufacturing costs of the PTC material (Table 1).

The thermally responsive polyethylene-carbon black (C@PE) composites through hot-rolling processing are prepared, selecting low-density polyethylene (LDPE) as the temperature-sensitive matrix due to its excellent compatibility with lithium-ion battery components. The process yields composites with varying carbon black contents (1, 5, 10, and 15 wt%), all exhibiting uniform filler distribution. Fig. 3a shows that increasing carbon content from 1% to 15% decreases room-temperature resistance from 55 Ω to 17.5 Ω while reducing the resistance increase ratio from 91.8 to 2.5. This phenomenon aligns with percolation theory - as CB loading increases beyond the percolation threshold, the probability of interparticle contact rises, facilitating the formation of continuous conductive pathways, thereby significantly reducing resistivity. However, this enhanced conductivity comes at the expense of diminished positive temperature coefficient (PTC) effect, as the densely interconnected CB network requires higher temperatures to achieve complete conductive pathway disruption. To enhance PTC performance, we incorporate thermoplastic polyurethane (TPU) into the 1% C@PE system. The resulting 1% TPU-1% C@PE composite demonstrates optimal characteristics, with resistance increasing from 78 Ω at room temperature to 10 380 Ω at 120 °C, achieving a maximum resistance increase

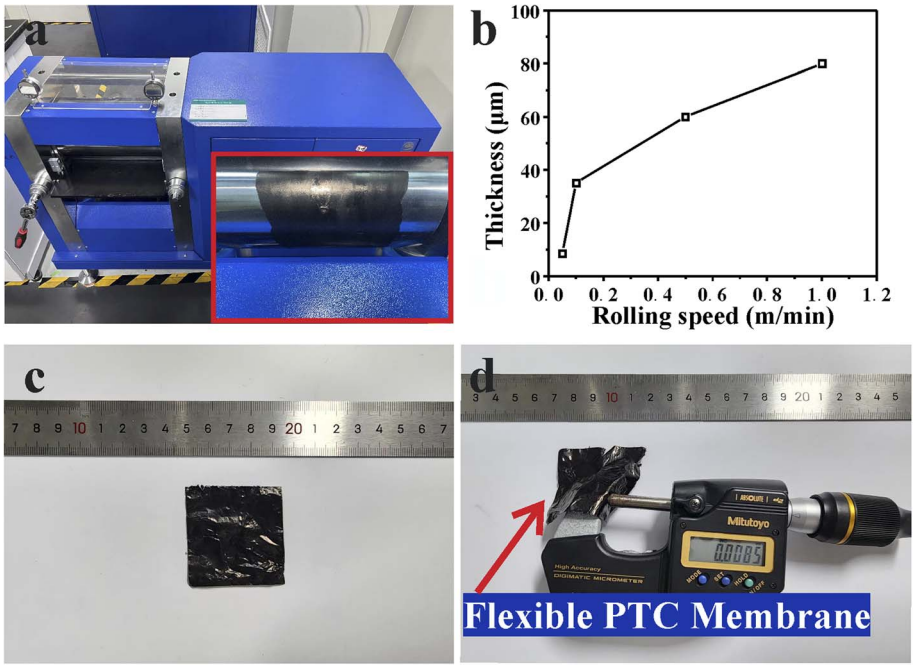

Fig. 2 (a) Preparation of PTC material using a heated roll mill (inset: schematic of the production process). (b) Thickness *versus* rolling speed. (c) Dimensions of the 1% TPU-1% C@PE composite. (d) Thickness of the 1% TPU-1% C@PE composite.

ratio of 133.1 (Fig. 3b). This improvement results from the differential thermal expansion between TPU and PE, which selectively disrupts the conductive network while maintaining adequate baseline conductivity at low TPU concentrations (≤1 wt%).

The SEM characterization reveals that all the samples maintain uniform filler distribution without agglomeration (Fig. 4a–d). For TPU-modified composites (Fig. 4e–h), the morphology remains stable across different TPU concentrations, with conductive networks preserving their homogeneous distribution. These solvent-free fabricated composites combine precise thickness control (achieving 8.5 μm) with balanced electrical-thermal response characteristics, representing a significant advancement over conventional solvent-based methods for battery safety applications. Fig. 4i shows the Raman spectra of composites with different TPU contents. It can be seen from the figure that conductive carbon black exhibits strong peaks at 1350 cm^{-1} (D peak, disordered carbon or sp^3 hybridization) and 1580 cm^{-1} (G peak, graphitization or sp^2 hybridization), while the characteristic peaks of polyethylene and TPU are weaker. With the increase of TPU content, the G peak shows a significant red shift, mainly due to the N–H bending vibration (~1530 cm^{-1}) in TPU. The optimized PE-MDI complex reveals that there is a weak charge transfer between the carbonyl oxygen atom of TPU and the hydrogen atom of PE, but no strong hydrogen bond is formed (2.870 or 2.899 Å), contributing 34.885 kJ mol^{-1} to the total interaction energy. Among various interaction visualization analysis methods, independent gradient model based on Hirshfeld partition (IGMH) has unique advantages in analyzing inter fragment interactions and is suitable for understanding the interaction between PE and TPU in this research work.[30,31] The optimized structure and related IGMH analysis results are shown in Fig. 4m. The IGMH analysis projects the sign (λ_2) ρ function onto the isosurface through different colors to display the type and intensity of interactions, as indicated by the color scale bars in the figure. Red indicates the presence of steric hindrance effects, green indicates the presence of van der Waals

Table 1 The comparison of positive temperature coefficient materials in previous thermal runaway preventing researches

PTC material	Solvent	Coating method	Thickness	Capacity retention	Ref.
LDPE + 20% Nickel particles	NMP	Casting	15 μm	~95% during 50 cycles	20
Epoxy + 40% carbon particle	Ethanol	Spreading	100 μm	N/A	24
PMMA + 10% carbon particle	Chloroform	Spreading	100 μm	N/A	23
PMMA + PVDF + 2.5% MWCNT	DMF	Blade coating	4 μm	~86.6% during 100 cycles @0.2 C	25
PVDF + 35% LFP particle	NMP	Spreading	4 μm	90% during 1350 cycles @1.0 C	28
EVA + 24% acetylene black	Petroleum ether	Spreading	10 μm	~99.60 during 100 cycles @0.5 C	26
LDPE + 9.1% Nickel particles	NMP	Blade coating	5 μm	95% during 5000 cycles @1 A g^{-1}	29
TPU + PE+1% conductive carbon black	Solvent free	Hot pressing	8.5 μm	98.2% during 250 cycles @5.0 C	This work

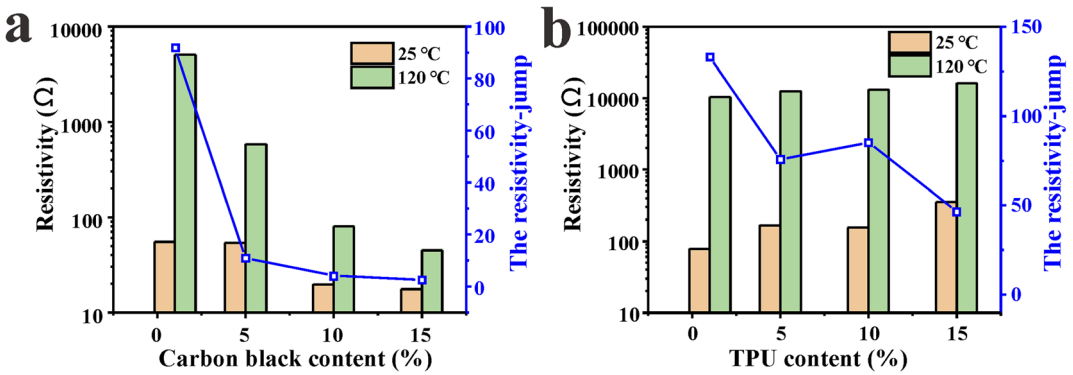

Fig. 3 Electrical properties of carbon-based composites: (a) C@PE with 1–15 wt% carbon black showing resistance and resistance increase ratio; (b) PE/CB composites with 1–15 wt% TPU (fixed 1 wt% CB content).

interactions, blue indicates significant attraction or ionic bonds, and complete blue indicates chemical bonds. The contour surfaces in Fig. 4m are all green, indicating that the interaction type between PE and TPU is van der Waals interaction. There is an obvious relationship between the PE-MDI complex. The van der Waals interaction in the composite ensure that the PE and TPU exhibit uniform dispersion behavior.

The charge/discharge behavior and cycling performance of both the 1% TPU-1% C@PE electrode battery and the reference battery under different C-rate conditions using a battery testing system are evaluated. The charge/discharge cutoff voltages are set at 3.75 V and 2.0 V, respectively. Fig. 5 demonstrates that the 1% TPU-1% C@PE electrode battery shows slightly lower discharge plateaus and slightly higher charge plateaus compared to the reference battery across all tested rates (0.1 C to 1.0 C), which are due to its marginally higher internal resistance. The voltage efficiencies for the 1% TPU-1% C@PE electrode battery measure 97.10%, 96.76%, 96.22%, and 95.39% at 0.1 C, 0.2 C, 0.5 C, and 1.0 C respectively, while the reference battery achieves 97.96%, 97.58%, 96.71%, and 96.39% at the same rates. Electrochemical impedance spectroscopy (EIS)

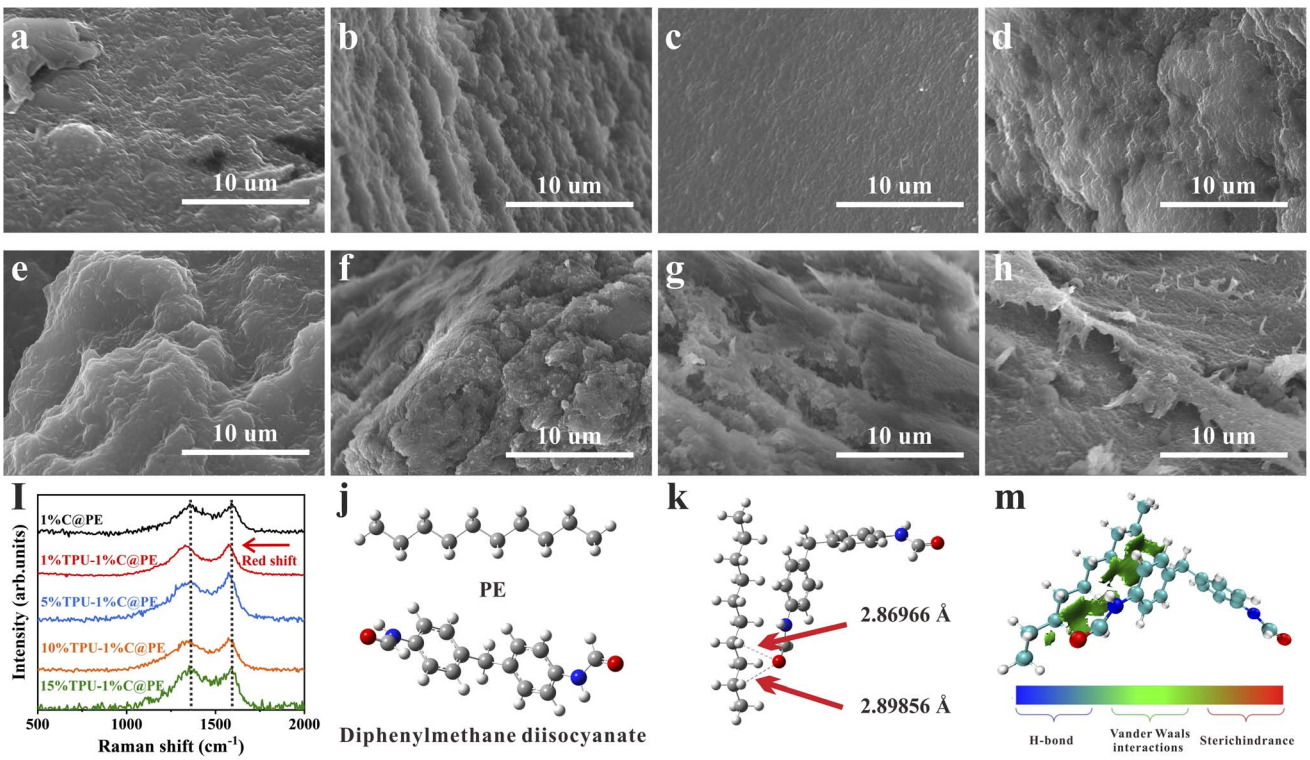

Fig. 4 Characterization of PE/CB composites: (a–d) with varying CB content (1–15 wt%); (e–h) with fixed 1 wt% CB and varying TPU content (1–15 wt%). (i) Raman spectra of TPU-reinforced composite. Optimized structures of: (j) PE segment (truncated alkane chain), (k) diphenylmethane diisocyanate monomer, and (m) PE-TPU complex.

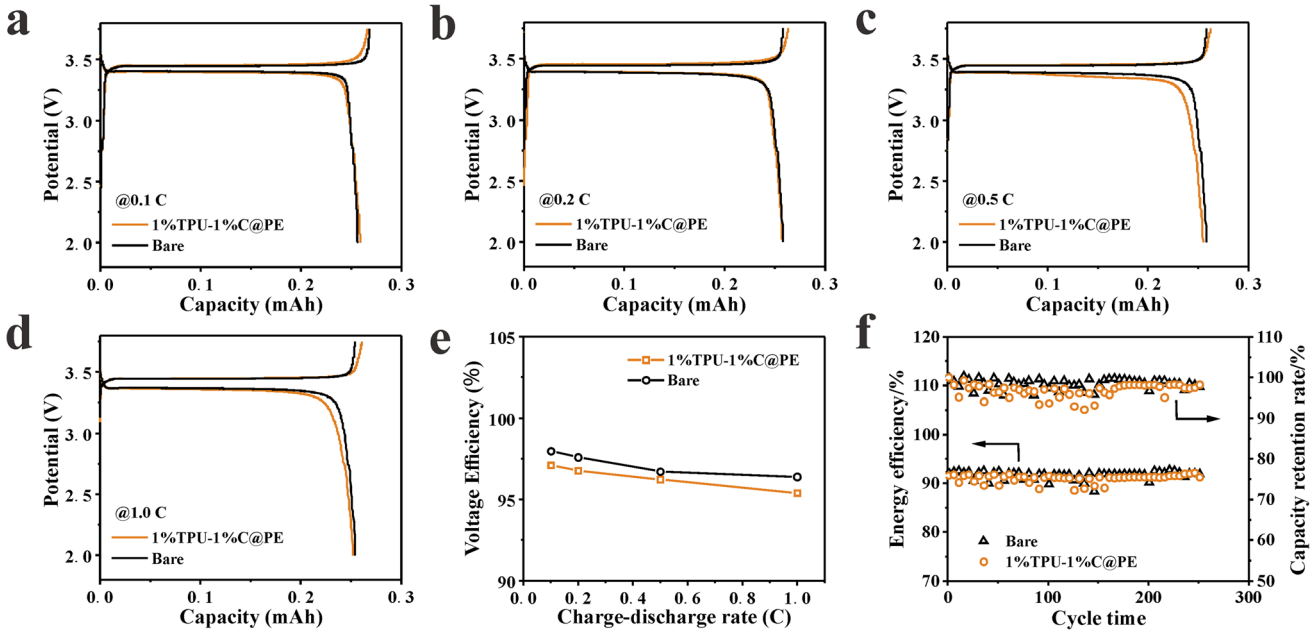

Fig. 5 Battery performance comparison between 1% TPU-1% C@PE composite and reference: (a–d) charge–discharge profiles at various C-rates; (e) voltage efficiency *versus* C-rate; (f) cycling stability.

analysis reveals the internal impedance characteristics of the 1% TPU-1% C@PE electrode battery, as shown in Fig. 6, revealing similar ohmic resistances for both batteries (4.26 Ω cm^2 *vs.* 4.22 Ω cm^2). The Nyquist plot consists of a depressed semicircle in the medium-high frequency region and a linear Warburg tail in the low frequency region. The equivalent circuit model inset in Fig. 6 includes R_b (bulk resistance), R_{ct} (charge transfer resistance), R-CEI and CPE-CEI (representing the resistance and constant phase element of the cathode electrolyte interface, respectively), along with W1 (Warburg impedance associated with lithium-ion diffusion). The fitting results demonstrate that the 1% TPU-1% C@PE electrode exhibits a slightly higher charge transfer resistance (78.76 Ω cm^{-2}) compared to the reference battery (70.76 Ω cm^{-2}), resulting in a 0.49% lower voltage efficiency at 0.5 C compared to the reference battery. These results confirm that voltage efficiency depends primarily on the battery's overall electronic resistance and reaction resistance.

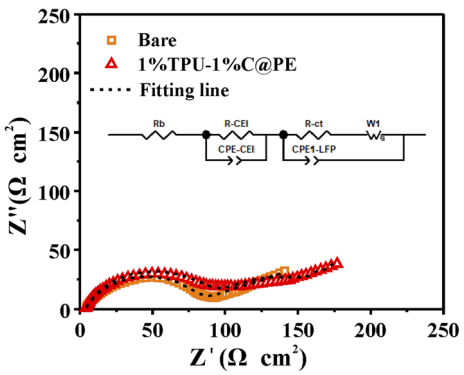

Fig. 6 Electrochemical impedance spectra of batteries with 1% TPU-1% C@PE and reference electrodes. (The black dashed line is the fitting line).

The cycling performance at 5 C current density (Fig. 5f) shows the 1% TPU-1% C@PE electrode battery maintains a 98.2% capacity retention rate (CRR) during 250 cycles, slightly outperforming the reference battery's 97.7%. This confirms that the 1% TPU-1% C@PE electrode preserves cycling stability. During high-rate operation, both batteries demonstrate comparable energy efficiencies (91.24% *vs.* 91.89%), further validating the practical viability of the 1% TPU-1% C@PE electrode.

A PTC effect test platform is constructed using a heating plate, LED circuit and PTC materials, with a 5.0 W LED powered by two series-connected batteries through 1% TPU-1% C@PE as the conductive pathway. The PTC intensity is evaluated by monitoring LED brightness changes under room temperature and 160 °C heating conditions. Experimental observations show that at room temperature, the 1% TPU-1% C@PE exhibits high conductivity, producing bright LED illumination. When subjected to 160 °C heating, the material demonstrates a sharp increase in electrical resistivity, leading to reduced circuit current and significantly dimmed LED brightness (Fig. 7). Upon returning to ambient conditions, the 1% TPU-1% C@PE's resistivity decreases markedly, restoring the circuit current and LED brightness to their original levels. This thermal-responsive behavior clearly demonstrates the effective PTC characteristics of the 1% TPU-1% C@PE composite material.

To evaluate the impact of the 1% TPU-1% C@PE material on battery thermal safety, a lithium iron phosphate/graphite coin battery incorporating this material is fabricated and charged to 100% state of charge (SOC)(Fig. 8). The 1% TPU-1% C@PE material layer, coated onto the carbon-coated aluminum foil

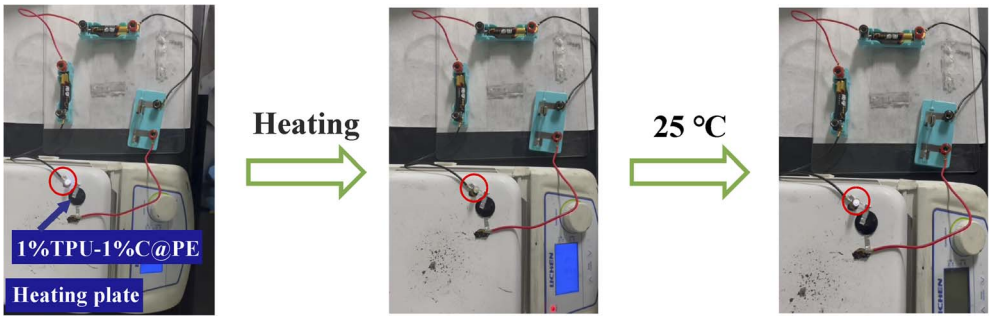

Fig. 7 Electrical resistivity *versus* temperature for 1% TPU-1% C@PE composite. The schematic inset illustrates the series circuit configuration with an LED indicator.

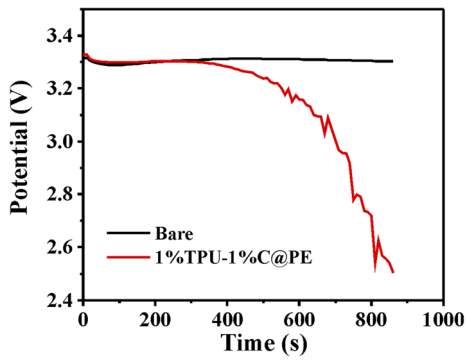

Fig. 8 The voltage cut-off behavior of 1% TPU-1% C@PE battery in 160 °C environment.

current collector, is designed to disrupt electron transport actively under elevated temperatures. During testing, the battery is discharged at 0.1 C and exposed to a constant ambient temperature of 160 °C. A high-temperature-resistant separator, capable of withstanding up to 180 °C, is employed to prevent internal short circuits caused by separator shrinkage or melting. Voltage measurements reveal that the initial open-circuit voltage of the 1% TPU-1% C@PE battery is 3.32 V, comparable to the 3.31 V of the reference cell, confirming consistent initial states. Under 160 °C heating, the reference cell voltage remains stable for 860 s, exhibiting only minor fluctuations attributable to ongoing discharge. In contrast, the voltage of the 1% TPU-1% C@PE cell begins to drop sharply after 290 s of heating and rapidly declines to 2.5 V by 860 s. This behavior is attributed to a rapid increase in the internal resistance resulting from the positive temperature coefficient (PTC) effect of the functional material, which actively interrupts the circuit and causes the voltage to collapse. These results demonstrate that the 1% TPU-1% C@PE material effectively induces an internal circuit-breaking mechanism under external heating, terminates electrochemical reactions, and significantly improves the thermal safety of lithium-ion batteries.

4. Conclusions

In summary, this study addresses lithium battery thermal safety by developing a novel PTC material based on TPU-reinforced PE/carbon composites. The solvent-free hot-rolling process successfully overcomes the limitations of conventional solution-casting methods, producing a uniform thin-film structure with a thickness of 8.5 μm. The optimized composite demonstrates rapid circuit interruption at the critical temperature of ~120 °C while maintaining a maximum resistance increase ratio of 133.1. Notably, the material exhibits excellent electrochemical compatibility, showing no adverse effects on charge/discharge behavior and a 98.2% capacity retention rate (CRR) during 250 cycles. The mechanism for reliable thermal protection attributes to the synergistic effect of TPU reinforcement and the precisely controlled conductive network, which ensures stable PTC switching performance. The open circuit voltage of 1% TPU-1% C@PE battery can quickly drop to 2.5 V within 570 s in an environment of 160 °C, due to the PTC effect of the material causing a rapid increase in internal resistance, thereby interrupting the circuit. This study provides an effective strategy for lithium battery thermal safety management, combining high performance with an environmentally friendly, cost-effective, and scalable fabrication process.

Conflicts of interest

There are no conflicts to declare.

Data availability

The data that support the findings of this study are available from the corresponding author upon reasonable request.

Acknowledgements

This work was supported by the Science and Technology Project of State Grid Corporation of China under Grant No. 5108-202218280A-2-76-XG.

References

1 G. liu, H. Hao, Z. Guo, J. Yang and W. Shen, *Energy Storage Mater.*, 2025, **76**, 104149.
2 C. Liu, L. Sheng and L. Jiang, *RSC Adv.*, 2025, **15**, 7995–8018.

3 T. Han, W. Cao, Z. Xu, V. Adibnia, M. Olgiati, M. Valtiner, L. Ma, C. Zhang, M. Ma, J. Luo and X. Banquy, *Sci. Adv.*, 2023, **9**, eadf3902.
4 J. Xiao, F. Shi, T. Glossmann, C. Burnett and Z. Liu, *Nat. Energy*, 2023, **8**, 329–339.
5 J. Xie and Y.-C. Lu, *Adv. Mater.*, 2025, **37**, 2312451.
6 G. Feng, L. Gao, J. Li, C. Zhang, Y. Wu, M. Tan, Q. Wang, F. Lv, L. Tao and M. Cao, *J. Alloy. Compd.*, 2025, **1022**, 179926.
7 Z. Jia, K. Jin, W. Mei, P. Qin, S. Jinhua and Q. Wang, *eTransportation*, 2025, **24**, 100390.
8 T. Tang, Q. Xia, M. Xu, Z. Deng, F. Jiang, Z. Wu, Y. Ren, D. Yang and C. Qian, *eTransportation*, 2025, **24**, 100406.
9 G. Chen, R. Tan, C. Zeng, Y. Li, Z. Zou, H. Wang, C. Ouyang, J. Wan and J. Yang, *Prog. Mater. Sci.*, 2025, **154**, 101516.
10 S. Ge, Y. Leng, T. Liu, R. S. Longchamps, X.-G. Yang, Y. Gao, D. Wang, D. Wang and C.-Y. Wang, *Sci. Adv.*, 2020, **6**, eaay7633.
11 C. Chen, R. Yang, J. Zhu, W. Yao and Y. Tang, *Adv. Sci.*, 2025, **12**, 2500756.
12 L. Zhou, L. Xie, J. Dai, A. Jain, G. Chen and Y. Zhao, *Asia-Pac. J. Chem. Eng.*, 2025, e70056.
13 L. Zhang, L. Wang, J. Zhang, Q. Wu, L. Jiang, Y. Shi, L. Lyu and G. Cai, *J. Energy Storage*, 2025, **112**, 115485.
14 L. Tong, Y. Li, Y. Xu, J. Fang, C. Wen, Y. Zheng, H. Zhang, B. Peng, F. Yang, J. Zhang and M. Gong, *J. Energy Storage*, 2025, **124**, 116843.
15 J. Yu, X. Sun, X. Shen, D. Zhang, Z. Xie, N. Guo and Y. Wang, *Energy Storage Mater.*, 2025, **76**, 104134.
16 H. Du, Y. Wang, Y. Kang, Y. Zhao, Y. Tian, X. Wang, Y. Tan, Z. Liang, J. Wozny, T. Li, D. Ren, L. Wang, X. He, P. Xiao, E. Mao, N. Tavajohi, F. Kang and B. Li, *Adv. Mater.*, 2024, **36**, 2401482.
17 C.-j. Wang, Y.-l. Zhu, T. Zhang, J. Tian, F. Gao, Y. Zhao, X.-y. Bu and T. Quan, *J. Clean. Prod.*, 2024, **470**, 143280.
18 I. T. Song, J. Kang, J. Koh, H. Choi, H. Yang, E. Park, J. Lee, W. Cho, Y.-m. Lee, S. Lee, N. Kim, M. Lee and K. Kim, *Nat. Commun.*, 2024, **15**, 8294.
19 S. Wang, S. Ma, L. Cao, Q. Li, Q. Ji, J. Huang, N. Lu, X. Xu, Y. Liu and J. Zhu, *J. Mater. Chem. C*, 2020, **8**, 11681–11686.
20 Z. Chen, P.-C. Hsu, J. Lopez, Y. Li, J. W. F. To, N. Liu, C. Wang, S. C. Andrews, J. Liu, Y. Cui and Z. Bao, *Nat. Energy*, 2016, **1**, 15009.
21 M. Li, G. Cai, J. Holoubek, K. Yu, H. Liu, S. Sarwar, Q. Yan, H. Gao, D. Zhang, H. Zhou, P. P. Mukherjee, S.-w. Lee, B.-y. Jung and Z. Chen, *Nano Energy*, 2022, **103**, 107726.
22 M. Li, Y. Shi, H. Gao and Z. Chen, *Adv. Funct. Mater.*, 2020, **30**, 1910328.
23 L. Xia, L. Zhu, H. Zhang and X. Ai, *Chin. Sci. Bull.*, 2012, **57**, 4205–4209.
24 X. M. Feng, X. P. Ai and H. X. Yang, *Electrochem. Commun.*, 2004, **6**, 1021–1024.
25 X. Zhang, C. Zhang, H. Li, Y. Cao, H. Yang and X. Ai, *ACS Appl. Energy Mater.*, 2022, **5**, 5236–5244.
26 H. Zhong, C. Kong, H. Zhan, C. Zhan and Y. Zhou, *J. Power Sources*, 2012, **216**, 273–280.
27 Y. Luo, C. Sang, K. Le, H. Chen, H. Li and X. Ai, *J. Energy Chem.*, 2024, **94**, 181–198.
28 H.-Z. Jin, X.-F. Han, P. M. Radjenovic, J.-H. Tian and J.-F. Li, *J. Phys. Chem. C*, 2021, **125**, 1761–1766.
29 W. Tian, Q. Gao, Y. Tan, K. Yang, L. Zhu, C. Yang and H. Zhang, *J. Mater. Chem. A*, 2015, **3**, 5656–5664.
30 T. Lu and Q. Chen, *J. Comput. Chem.*, 2022, **43**, 539–555.
31 T. Lu, *J. Chem. Phys.*, 2024, **161**, 082503.